Inorg. Chem. **1996,** *35,* 5885−5892

Structural and Resonance Raman Studies of an Oxygen-Evolving Catalyst. Crystal Structure of $[(bpy)_2(H_2O)Ru^{III}ORu^{IV}(OH)(bpy)_2](ClO_4)_4$

Jon R. Schoonover,* JinFeng Ni, Lee Roecker, Peter S. White, and Thomas J. Meyer*

Bioscience/Biotechnology Group, Mail Stop J586, Chemical Science and Technology Division, Los Alamos National Laboratory, Los Alamos, New Mexico 87545, and Department of Chemistry, Kenan and Venable Laboratories, The University of North Carolina at Chapel Hill, Chapel Hill, North Carolina 27599-3290

Received March 29, 1996[⊗]

The oxidized form of the blue dimer water oxidation catalyst $[(bpy)_2(H_2O)Ru^{III}ORu^{IV}(OH)(bpy)_2](ClO_4)_4$ (bpy is 2,2′-bipyridine) has been characterized structurally by X-ray crystallography. Comparisons with $[(bpy)_2(H_2O)Ru^{III}ORu^{III}(OH_2)(bpy)_2](ClO_4)_4\cdot 2H_2O$, $[(bpy)_2ClRu^{III}ORu^{IV}Cl(bpy)_2](ClO_4)_3\cdot H_2O$, and $[(tpy)(bpy)Os^{III}OOs^{IV}(bpy)(tpy)]Na(ClO_4)_6\cdot 3H_2O$ (tpy is 2,2′:6′,2″-terpyridine) reveal that oxidation of $Ru^{III}-O-Ru^{III}$ to $Ru^{III}-O-Ru^{IV}$ results in significant structural changes at the μ-oxo bridge. There is an increase toward linearity along M−O−M, a decrease in the M−O bond distances at the bridge, and an increase in the $H_2O-Ru-O$ bridge angle. These changes are discussed in the context of the structural requirements for O···O coupling and O_2 evolution in higher oxidation states. Resonance Raman spectra of these and related complexes reveal that internal ligand vibrations as well as overtone and combination bands of an intense, symmetrical M−O−M stretch at 360−400 cm^{-1} contribute significantly to the Raman spectra. Additional M−O−M bands are identified near 800 cm^{-1} and, tentatively, near 130 cm^{-1}. It is not possible to assign bands to $Ru-OH_2$ or Ru−OH stretches; bands at low energy appear to originate from modes that are highly mixed.

Photosynthesis by oxygen-evolving organisms depends on the interplay of two photosystems. Photosystem II is responsible for the light-driven oxidation of water to dioxygen and the transfer of electrons to photosystem I. In photosystem II there is a light-harvesting complex, a core with a reaction center, and a site for water oxidation. Mechanistic and structural investigations of photosynthetic O_2 evolution are complicated by the inherent chemical complexity of the system. A manganese tetranuclear cluster is believed to be the oxygen-evolving catalyst, and significant effort has been devoted to the study of model systems for the active site.[1] Although many manganese model complexes have been synthesized, only recently was stoichiometric or catalytic reactivity toward water demonstrated in the case of a linked porphyrin complex.[2,3]

A useful functional model for water oxidation is the blue dimer $[(bpy)_2(H_2O)Ru^{III}ORu^{III}(OH_2)(bpy)_2]^{4+}$ (bpy is 2,2′-bipyridine).[4] From the results of X-ray crystallography on the salt $[(bpy)_2(H_2O)Ru^{III}ORu^{III}(OH_2)(bpy)_2](ClO_4)_4\cdot 2H_2O$, each Ru site is coordinated to two 2,2′-bipyridine ligands, the oxygen of a coordinated water, and a bridging oxo. The Ru−O−Ru angle is 165°. The initial form as $Ru^{III}-O-Ru^{III}$ can be oxidized chemically or electrochemically in a series of stepwise reactions in which electrons and protons are lost, ultimately to give $Ru^{V}-O-Ru^{V}$, presumably as $[(bpy)_2(O)Ru^{V}ORu^{V}(O)(bpy)_2]^{4+}$. The net effect of the loss of 4 electrons and 4 protons matches the requirements for water oxidation ($2H_2O \rightarrow O_2 + 4H^+ + 4e^-$), and there is adequate driving force in the $Ru^{V}-Ru^{V}/Ru^{III}-Ru^{III}$ couple (1.53 V) to effect the reaction.

The results of $H_2{}^{18}O$-labeling studies suggest that at least some of the O_2 produced comes from the bound waters and the mechanism of O···O coupling may involve the two oxo atoms in $[(bpy)_2(O)Ru^{V}ORu^{V}(O)(bpy)_2]^{4+}$.[5] In any case, the structure of the μ-oxo−diaqua framework is a key element in the reactivity of the ion. Hurst et al. have utilized resonance Raman spectroscopy to gain vibrational information including results on higher oxidation states.[6] The study focused mainly on the frequency of the symmetrical Ru−O−Ru stretch and the effect of ^{18}O isotopic substitution.

* Corresponding authors: J.R.S., Los Alamos National Laboratory; T.J.M., The University of North Carolina at Chapel Hill.

⊗ Abstract published in *Advance ACS Abstracts*, September 1, 1996.

(1) (a) Govindjee, T.; Coleman, W. *Photochem. Photobiol.* **1985**, *42*, 187. (b) Amesz, J. *Biochim. Biophys. Acta* **1983**, *726*, 1. (c) Renger, G. *Angew. Chem.* **1987**, *26*, 643. (d) George, G. N.; Prince, R. C.; Cramer, S. P. *Science* **1989**, *243*, 789. (e) Brudvig, G. W., Crabtree, R. H. *Proc. Natl. Acad. Sci. U.S.A.* **1986**, *83*, 4586. (f) Bocarsly, J. R.; Brudvig, G. W. *J. Am. Chem. Soc.* **1992**, *114*, 9762. (g) Koulougliotis, D.; Hirsh, D. J.; Brudvig, G. W. *J. Am. Chem. Soc.* **1992**, *114*, 8322. (h) Proserpio, D. M.; Hoffmann, R.; Dismukes, G. C. *J. Am. Chem. Soc.* **1992**, *114*, 4374.

(2) (a) Christou, G. *Acc. Chem. Res.* **1989**, *22*, 328. (b) Pecoraro, V. L. *Photochem. Photobiol.* **1988**, *48*, 249. (c) Wieghardt, K. *Angew. Chem.* **1989**, *28*, 1153. (d) Brudvig, G. W. Crabtree, R. H. *Prog. Inorg. Chem.* **1989**, *37*, 99. (e) Vincent, J. B.; Christou, G. *Adv. Inorg. Chem.* **1989**, *33*, 197. (f) Sarneski, J. E.; Brzezinski, L. J.; Anderson, B.; Didiuk, M.; Manchanda, R.; Crabtree, R. H.; Brudvig, G. W.; Schulte, G. K. *Inorg. Chem.* **1993**, *32*, 3265. (g) Dave, B. C.; Czernuszewicz, R. S.; Bond, M. R.; Carrano, C. J. *Inorg. Chem.* **1993**, *32*, 3593. (h) Reddy, K. R.; Rajasekharan, M. V.; Padhye, S.; Dahan, F.; Tuchagues, J. P. *Inorg. Chem.* **1994**, *33*, 428. (i) Ashamawy, F. M.; McAuliffe, C. A.; Parish, R. V.; Tames, J. *J. Chem. Soc., Dalton Trans.* **1985**, 1391. (j) Ramaraj, R.; Kira, A.; Kaneko, M. *Angew. Chem.* **1986**, *25*, 825. (k) Yao, G. J.; Kira, A.; Kaneko, M. *J. Chem. Soc., Faraday Trans.* **1988**, *84*, 4451.

(3) Naruta, Y.; Sasayama, M.; Sasaki, T. *Angew. Chem., Int. Ed. Engl.* **1994**, *33*, 1839.

(4) (a) Gilbert, J. A.; Eggleston, D. S.; Murphy, W. R., Jr.; Geselowitz, D. A.; Gersten, S. W.; Hodgson, D. J.; Meyer, T. J. *J. Am. Chem. Soc.* **1985**, *107*, 3855. (b) Comte, P.; Nazeeruddin, M. K.; Rotzinger, F. P.; Frank, A. J.; Gratzel, M. *J. Mol. Catal.* **1989**, *52*, 63. (c) Rotzinger, F. P.; Munavalli, S.; Comte, P.; Hurst, J. K.; Gratzel, M.; Pern, F.-J.; Frank, A. J. *J. Am. Chem. Soc.* **1987**, *109*, 6619. (d) Lei, Y. B.; Hurst, J. K. *Inorg. Chim. Acta* **1994**, *226*, 179.

(5) Geselowitz, D.; Meyer, T. J. *Inorg. Chem.* **1990**, *29*, 3894.

(6) (a) Hurst, J. K.; Zhou, J.; Lei, Y. B. *Inorg. Chem.* **1992**, *31*, 1010. (b) Lei, Y. B.; Hurst, J. K. *Inorg. Chem.* **1994**, *33*, 4460.

S0020-1669(96)00348-5 CCC: $12.00

Table 1. Crystallographic Data for $[(bpy)_2(H_2O)Ru^{III}ORu^{IV}(OH)(bpy)_2](ClO_4)_4\cdot 2H_2O$ ($(H_2O)Ru^{III}ORu^{IV}(OH)$) Compared to $[(bpy)_2(Cl)Ru^{III}ORu^{IV}(Cl)(bpy)_2](ClO_4)_3\cdot H_2O$ ($(Cl)Ru^{III}ORu^{IV}(Cl)$) and $[(tpy)(bpy)Os^{III}OOs^{IV}(bpy)(tpy)]Na(ClO_4)_6\cdot 3H_2O$ ($(bpy)Os^{III}OOs^{IV}(bpy)$)

	$(H_2O)Ru^{III}ORu^{IV}(OH)$	$(Cl)Ru^{III}ORu^{IV}(Cl)$	$(bpy)Os^{III}OOs^{IV}(bpy)$
formula	$Ru_2C_{40}H_{39}C_{14}N_8O_{21}$	$Ru_2C_{40}H_{34}C_{14}N_8O_{14}Cl_2$	$Os_2NaC_{50}H_{44}Cl_6N_{10}O_{28}$
space group	$P2_1/n$	$P2_1/c$	$P1$
a, Å	13.721(14)	18.297(6)	13.235(5)
b, Å	20.44(4)	11.939(14)	18.074(1)
c, Å	17.172(25)	21.447(9)	13.088(6)
α, deg			90.57(4)
β, deg	93.38(10)	95.08(4)	91.83(4)
γ, deg			95.72(4)
V, Å^3	4804(12)	4666.5	3113.3
d_{calcd}, g/cm^3	1.802	1.75	1.99
Z	4	4	2
crystal size, mm	0.30 × 0.30 × 0.40	0.24 × 0.02 × 0.30	0.35 × 0.30 × 0.30
λ(Mo Kα), Å	0.709 30	0.7107	0.7107
R	0.103	0.077	0.056
R_w	0.120	0.064	0.054

In this paper, we add spectroscopic and structural information about this important model system by presenting crystal structure data for the higher oxidation state salt $[(bpy)_2(H_2O)Ru^{III}ORu^{IV}(OH)(bpy)_2](ClO_4)_4$ and resonance Raman data for $[(bpy)_2(H_2O)Ru^{III}ORu^{III}(OH_2)(bpy)_2]^{4+}$, $[(phen)_2(H_2O)Ru^{III}ORu^{III}(OH_2)(phen)_2]^{4+}$ (phen is 1,10-phenanthroline), $[(bpy)_2(H_2O)Ru^{III}ORu^{IV}(OH)(bpy)_2]^{4+}$, the related hydroxide, chloride, or acetonitrile derivatives, and the osmium μ-oxo complexes $[(bpy)_2(H_2O)Os^{III}OOs^{IV}(OH_2)(bpy)_2]^{5+}$ and $(tpy)(bpy)Os^{III}OOs^{IV}(bpy)(tpy)]^{5+}$. These data will be useful for future studies based on the M−O−M core.

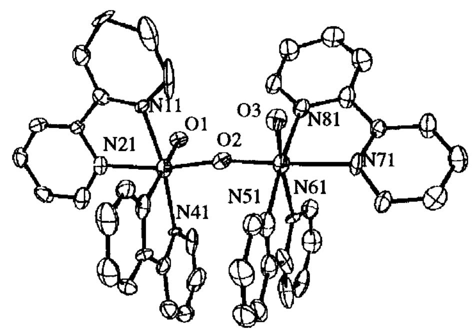

Figure 1. ORTEP drawing of $[(bpy)_2H_2O)Ru^{III}ORu^{IV}(OH)(bpy)_2](ClO_4)_4$.

Experimental Section

Preparations. $[(bpy)_2(H_2O)Ru^{III}ORu^{III}(OH_2)(bpy)_2](ClO_4)_4\cdot 2H_2O$, $[(bpy)_2ClRu^{III}ORu^{III}Cl(bpy)_2](ClO_4)_2$, and $[(bpy)_2(H_2O)Os^{III}OOs^{IV}(OH_2)(bpy)_2](ClO_4)_5$ were prepared according to published methods.[4a,7] The various hydroxy derivatives were prepared by dissolution of the aqua complex in the desired buffer solution. The acetonitrile complexes were prepared by dissolving the aqua complex in CH_3CN and allowing the solution to sit for 24 h.

Warning. Perchlorate salts are hazardous because of the possibility of explosion. They should be prepared in small amounts and stored appropriately.

$[(bpy)_2(H_2O)Ru^{III}ORu^{IV}(OH)(bpy)_2](ClO_4)_4$. To a 4 mL H_2O solution of $[(bpy)_2(H_2O)Ru^{III}ORu^{III}(H_2O)(bpy)_2](ClO_4)_4$ (0.03 g, 0.023 mmol) was added 0.47 mL of 0.05 M $Ce(ClO_4)_4$. The solution was stirred for 30 min, and saturated $NaClO_4$ was added dropwise to precipitate $[(bpy)_2(H_2O)Ru^{III}ORu^{IV}(OH)(bpy)_2](ClO_4)_4$. The product was collected on a frit, washed with 2 mL of ice-cold water, and dried under vacuum. The yield was 72%.

$[(phen)_2(H_2O)Ru^{III}ORu^{III}(OH_2)(phen)_2][ClO_4]_4$. Essentially the same procedure was used as in the preparation of $[(bpy)_2(H_2O)Ru^{III}ORu^{III}(OH_2)(bpy)_2][ClO_4]_4$. Higher yields resulted by avoiding light while solutions were heated to reflux. The complex $Ru(phen)_2Cl_2$ (0.5 g, 0.939 mmol)[8] was dissolved in 10 mL of water and the resulting solution heated to reflux. A solution of $AgNO_3$ (0.399 g, 2.35 mmol) in 5 mL of water was added, and the resulting solution was heated at reflux for 45 min. The solution was cooled to room temperature and the AgCl filtered off with a fine frit. A saturated solution of $NaClO_4$ (about 1 mL) was added slowly until most of the solid precipitated. The dark solid was isolated, washed with 5 mL of cold water, and dried under vacuum for 1 h. The yield was 45%.

For recrystallization, the crude product was dissolved in a minimum amount of water, several drops of saturated $NaClO_4$ were added, and the solution was shaken. This process was repeated several times until the green solid was completely precipitated. The solution was filtered and the filtrate kept at room temperature overnight. The crystalline product was isolated, washed with 2 mL of cold water, and dried under vacuum. The yield was 18%.

X-ray Crystallography. Crystals of $[(bpy)_2(H_2O)Ru^{III}ORu^{IV}(OH)(bpy)_2](ClO_4)_4\cdot 2H_2O$ were obtained at room temperature from a saturated solution containing $NaClO_4$. Intensity data were collected by the $\theta-2\theta$ scan mode in the range $4° < 2\theta < 45°$ on a Nonius diffractometer with Mo Kα radiation, $\lambda = 0.709\ 30$ Å. A total of 5857 unique data were collected over the following h, k, and l ranges: −12 to 12, 0 to 22, 0 to 18. The structure was solved by direct methods and was refined by full-matrix, least-squares methods to yield final R and R_w values of 0.103 and 0.120 for 676 variables and 3759 observations with $I > 2.5\sigma(I)$. The ClO_4^- anions appear to be disordered (i.e. the O thermal parameters were extremely large). However, no disorder model resulted in a significant improvement. The disorder of the counteranions leads to the high R values. Some data collection parameters are listed in Table 1, while complete description of the parameters, structure solution and refinement conditions, atomic coordinates, bond distances and angles, and thermal parameters are provided as Supporting Information.

Resonance Raman Spectra. Resonance Raman spectra were recorded at the UNC Laser Facility. Laser excitation at 647.1 nm was provided by a Coherent Innova 90K Kr^+ laser, while excitation at 514.5 or 488.0 nm was provided by a Spectra-Physics 165 Ar^+ laser. The scattered radiation was dispersed by a Jobin Yvon U1000 double monochromator and detected by a Hamamatsu R943-02 cooled photomultiplier tube with signal processing by an Instruments SA Spectra Link photon-counting system. The spectra are typically the average of four to nine accumulations. The spectral resolution is 4 cm^{-1}.

Results

Crystal Structure. Crystals of $[(bpy)_2(H_2O)Ru^{III}ORu^{IV}(OH)(bpy)_2](ClO_4)_4$ are dark orange. The structure of the cation is shown in Figure 1. Selected bond distances and angles are listed in Table 2. The two Ru atoms are bridged by an oxygen atom. Each Ru center is approximately octahedrally coordinated by two bipyridine ligands (bpy), the bridging oxo atom, and

(7) (a) Weaver, T. R.; Meyer, T. J.; Adeyemi, S. A.; Brown, G. M.; Eckberg, R. P.; Hatfield, W. E.; Johnson, E. C.; Murray, R. W.; Untereker, D. *J. Am. Chem. Soc.* **1975**, *97*, 3039. (b) Gilbert, J. A.; Geselowitz, D.; Meyer, T. J. *J. Am. Chem. Soc.* **1986**, *108*, 1493. (c) Raven, S. R.; Meyer, T. J. *Inorg. Chem.* **1988**, *27*, 4478.
(8) Godwin, J. B.; Meyer, T. J. *Inorg. Chem.* **1971**, *10*, 471.

Table 2. Selected Bond Distances (Å) and Angles (deg) for $[(bpy)_2(H_2O)Ru^{III}ORu^{IV}(OH)(bpy)_2](ClO_4)_4.2H_2O$ Based on the Labeling Scheme in Figure 1

Ru(1)−O(1)	2.148(11)	Ru(2)−O(2)	1.978(14)
Ru(1)−O(3)	1.847(12)	Ru(2)−O(3)	1.823(12)
Ru(1)−N(11)	2.072(15)	Ru(2)−N(51)	2.059(15)
Ru(1)−N(21)	2.053(13)	Ru(2)−N(61)	2.122(14)
Ru(1)−N(31)	2.019(14)	Ru(2)−N(71)	2.105(13)
Ru(1)−N(41)	2.100(14)	Ru(2)−N(81)	2.085(14)
O(1)−Ru(1)−O(3)	94.7(5)	O(2)−Ru(2)−O(3)	99.2(5)
O(1)−Ru(1)−N(11)	89.4(5)	O(2)−Ru(2)−N(51)	91.5(6)
O(1)−Ru(1)−N(21)	84.8(5)	O(2)−Ru(2)−N(61)	165.2(5)
O(1)−Ru(1)−N(31)	171.0(6)	O(2)−Ru(2)−N(71)	86.7(6)
O(1)−Ru(1)−N(41)	92.7(5)	O(2)−Ru(2)−N(81)	87.9(6)
O(3)−Ru(1)−N(11)	92.4(5)	O(3)−Ru(2)−N(51)	90.8(5)
O(3)−Ru(1)−N(21)	169.6(6)	O(3)−Ru(2)−N(61)	89.8(5)
O(3)−Ru(1)−N(31)	91.9(5)	O(3)−Ru(2)−N(71)	170.5(5)
O(3)−Ru(1)−N(41)	96.1(5)	O(3)−Ru(2)−N(81)	93.9(5)
N(11)−Ru(1)−N(21)	77.2(6)	N(51)−Ru(2)−N(61)	76.6(6)
N(11)−Ru(1)−N(31)	96.6(6)	N(51)−Ru(2)−N(71)	96.4(6)
N(11)−Ru(1)−N(41)	171.0(5)	N(51)−Ru(2)−N(81)	175.3(5)
N(11)−Ru(1)−N(31)	96.6(6)	N(51)−Ru(2)−N(71)	96.4(6)
N(11)−Ru(1)−N(41)	171.0(5)	N(51)−Ru(2)−N(81)	175.3(5)
N(21)−Ru(1)−N(31)	89.8(5)	N(61)−Ru(2)−N(71)	86.1(6)
N(21)−Ru(1)−N(41)	94.2(6)	N(61)−Ru(2)−N(81)	103.3(6)
N(31)−Ru(1)−N(41)	80.5(6)	N(71)−Ru(2)−N(81)	78.7(5)
Ru(1)−O(3)−Ru(2)	170.0(7)		

the oxygen atom of a coordinated water molecule or a hydroxide anion. The two bpy ligands at each Ru center are arranged in the cis geometry. The coordinating atoms in the equatorial positions are bent away slightly from the bridging oxygen atom. The important bond distances and angles for this complex are compared to the analogous distances and angles for $[(bpy)_2(H_2O)Ru^{III}ORu^{III}(OH_2)(bpy)_2](ClO_4)_4{\cdot}2H_2O$, $[(bpy)_2ClRu^{III}ORu^{IV}Cl(bpy)_2](ClO_4)_3{\cdot}H_2O$, and $(tpy)(bpy)Os^{III}OOs^{IV}(bpy)(tpy)]Na(ClO_4)_6{\cdot}3H_2O$ in Table 3.[9]

Resonance Raman Spectra. Low-energy resonance Raman spectra of $[(bpy)_2(H_2O)Ru^{III}ORu^{III}(OH_2)(bpy)_2]^{4+}$ at pH = 1, $[(bpy)_2ClRu^{III}ORu^{III}Cl(bpy)_2]^{2+}$ at pH = 1, and $[(bpy)_2(CH_3CN)Ru^{III}ORu^{III}(NCCH_3)(bpy)_2]^{2+}$ in CH_3CN are compared in Figure 2. In Figure 3 are shown spectra for $[(phen)_2(H_2O)Ru^{III}ORu^{III}(OH_2)(phen)_2]^{4+}$ (pH = 0) and $[(phen)_2(HO)Ru^{III}ORu^{III}(OH)(phen)_2]^{2+}$ (pH = 7). The spectra were measured at room temperature in buffered aqueous solutions with excitation (647.1 nm) into the intense absorption band near 640 nm.[7a] Raman band energies for these complexes with proposed assignments are listed in Table 4.

The spectrum of $[(bpy)_2(H_2O)Ru^{III}ORu^{III}(OH_2)(bpy)_2]^{4+}$ is typical of μ-oxo $Ru^{III}-Ru^{III}$ complexes with an intense band appearing at 384 cm^{-1} and 14 additional medium-intensity bands between 100 and 500 cm^{-1}. The intense 384-cm^{-1} band has been assigned as the symmetrical Ru−O−Ru stretch (ν_s(Ru−O−Ru)).[6] Above 500 cm^{-1}, weak overtones and combinations associated with ν_s(Ru−O−Ru) are observed as are bands attributed to the ring modes of bpy. Near-resonance Raman excitation at 514.5 nm (Figure 4) demonstrates that the intense feature at 384 cm^{-1} is a convolution of an intense band at 383 cm^{-1} and weaker shoulders at 368 and 401 cm^{-1}. The intensities of the bpy bands are notably enhanced with higher energy excitation.

Raising the pH from 1 to 7 results in $[(bpy)_2(HO)Ru^{III}ORu^{III}(OH)(bpy)_2]^{2+}$ as the dominant form in solution.[4a] A slight shift from 384 to 382 cm^{-1} occurs for ν_s(Ru−O−Ru), but otherwise the spectra are nearly identical. In the Raman spectrum of $[(bpy)_2ClRu^{III}ORu^{III}Cl(bpy)_2]^{2+}$, as compared to the aqua and hydroxy complexes, new bands are observed at 120, 321, and 441 cm^{-1} and ν_s(Ru−O−Ru) shifts to 380 cm^{-1}.

The same general pattern of Raman bands is evident in the low-energy region with 1,10-phenanthroline (phen) rather than 2,2′-bipyridine (bpy) as the ancillary ligand in the μ-oxo structure (Figure 3), but energy shifts are observed. Bands are observed at 180, 339, and 461 cm^{-1} for the phen complexes which can be assigned to phen modes by comparison to resonance Raman spectra of $[Ru(phen)_3]^{2+}$. Raman bands for the bpy complexes at 133, 239, 254, 300, 419, and 485 cm^{-1} appear at 129, 236, 267, 306, 429, and 495 cm^{-1} for the phen complexes. These energy differences suggest some influence of the polypyridyl ligands on the Raman bands in this region. Between 500 and 1000 cm^{-1} Raman bands associated with combination modes of ν_s(Ru−O−Ru) and the first overtone are also observed. Bands associated with the ring modes of the phen ligand are also evident at higher energy.

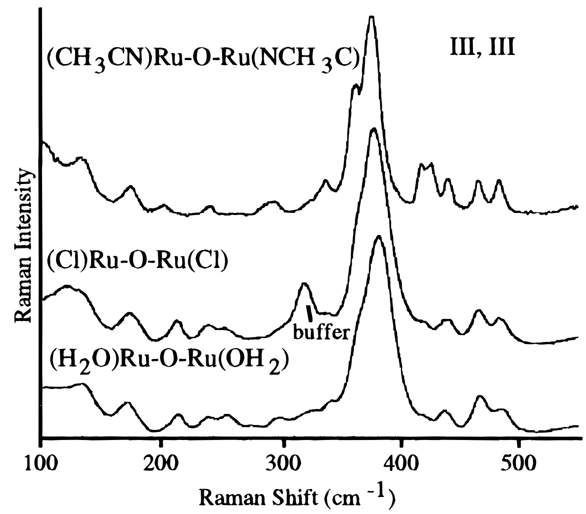

Figure 2. Low-energy resonance Raman spectra of $[(bpy)_2(H_2O)Ru^{III}ORu^{III}(OH_2)(bpy)_2]^{4+}$ in H_2O/triflic acid, pH = 1, $[(bpy)_2(Cl)Ru^{III}ORu^{III}(Cl)(bpy)_2]^{2+}$ in H_2O/triflic acid, pH = 1, and $[(bpy)_2CH_3CN)Ru^{III}ORu^{III}(NCCH_3)(bpy)_2]^{4+}$ in CH_3CN. The spectra were measured with 647.1 nm excitation and are the sum of between 4 and 16 coadded scans. The spectra were obtained in solution at room temperature with a spinning sample cell. Raman band energies are listed in Table 4.

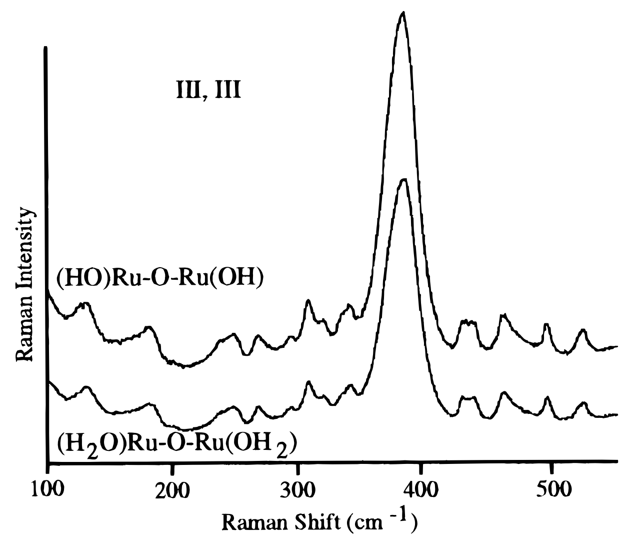

Figure 3. Low-energy resonance Raman spectra of $[(phen)_2(HO)Ru^{III}ORu^{III}(OH)(phen)_2]^{2+}$ (phosphate buffer, pH = 7) and $[(phen)_2(H_2O)Ru^{III}ORu^{III}(OH_2)(phen)_2]^{4+}$ (1 M triflic acid, pH = 0). The conditions were as in Figure 2. Raman band energies are listed in Table 4.

(9) Roecker, L. E. Ph.D. dissertation, The University of North Carolina at Chapel Hill, 1983.

Table 3. Comparison of Important Bond Distances (Å) and Angles (deg) in $[(bpy)_2(H_2O)Ru^{III}ORu^{III}(OH_2)(bpy)_2](ClO_4)_4 \cdot 2H_2O$ $[(bpy)_2(H_2O)Ru^{III}ORu^{IV}(OH)(bpy)_2](ClO_4)_4 \cdot 2H_2O$, $[(bpy)_2ClRu^{III}ORu^{IV}Cl(bpy)_2](ClO_4)_3 \cdot H_2O$, and $[(tpy)(bpy)Os^{III}OOs^{IV}(bpy)(tpy)](ClO_4)_6Na \cdot 3H_2O$

	$(H_2O)Ru^{III}ORu^{III}(OH_2)$	$(H_2O)Ru^{III}ORu^{IV}(OH)$	$ClRu^{III}ORu^{IV}Cl$	$Os^{III}OOs^{IV}$
		Distances		
M(1)−O	1.869(1)	1.847(12)	1.845(9)	1.861(8)
M(2)−O	1.869(1)	1.823(12)	1.805(9)	1.877(8)
L−M(1)	2.136(4) (L = H_2O)	2.148(11) (L = H_2O)	2.357(4) (L = Cl^-)	
M(2)−L′	2.136(4) (L′ = H_2O)	1.978(14) (L′ = OH^-)	2.339(4) (L′ = Cl^-)	
L···L′ [a]	4.725(5) ($H_2O \cdots OH_2$)	5.555(2) ($H_2O \cdots OH$)	5.777(5) (Cl···Cl)	
		Angles		
L−M(1)−O	89.4(2) (L = H_2O)	94.7(5) (L = H_2O)	95.1(3) (L = Cl^-)	
O−M(2)−L′	89.4(2) (L′ = H_2O)	99.2(5) (L′ = OH^-)	93.6(3) (L′ = Cl^-)	
M(1)−O−M(2)	165.4(3)	170.0(7)	170.7(5)	169.0(5)
L−M(1)−M(2)−L′ [b]	65.7 ($H_2O \cdots OH_2$)	117.2 ($H_2O \cdots OH$)	117.0 (Cl···Cl)	

[a] Distance of separation between adjacent cis ligands across the μ-oxo bridge. [b] Torsional angle of L, L′ along the direct M(1)−M(2) axis.

Dissolving solid $[(bpy)_2(H_2O)Ru^{III}ORu^{III}(OH_2)(bpy)_2](ClO_4)_4$ in acetonitrile results in complete replacement of the aqua ligands with solvent molecules after ca. 24 h.[10] In resonance Raman spectra of $[(bpy)_2(CH_3CN)Ru^{III}ORu^{III}(NCCH_3)(bpy)_2]^{4+}$ and $[(phen)_2(CH_3CN)Ru^{III}ORu^{III}(NCCH_3)(phen)_2]^{4+}$, bands below 500 cm^{-1} are narrowed relative to those of the aqua complexes and ν_s(Ru−O−Ru) shifts to lower energy. Major changes in the spectrum of the bpy complex include a new band at 428 cm^{-1} along with gains in relative intensity for bands at 339 and 419 cm^{-1}. The band at 213 cm^{-1} and the doublet near 300 cm^{-1} for the aqua complex both shift by about 10 cm^{-1} to lower energy.

No significant isotopic shifts were observed upon incubation of $[(bpy)_2(H_2O)Ru^{III}ORu^{III}(OH_2)(bpy)_2]^{4+}$ in $D_2{}^{16}O$ or $H_2{}^{18}O$ consistent with earlier results.[6] Spectral subtractions do show slight derivative shapes at the intense band near 385 cm^{-1} and for the band near 800 cm^{-1}, but there are no other notable differences. Spectra for $[Ru(tpy)(bpy)(OH_2)]^{2+}$ (tpy is 2,2′:6′,2″-terpyridine) in $H_2{}^{16}O$, $D_2{}^{16}O$, or $H_2{}^{18}O$ were measured with 457.9-nm excitation and show no measurable isotopic effects as well.

Changes are observed in the Raman spectrum of $[(bpy)_2(H_2O)Ru^{III}ORu^{IV}(OH_2)(bpy)_2]^{5+}$ by raising the pH from 0 to 2 to 7, but they are slight. ν_s(Ru−O−Ru) shifts from 392 to 389 to 386 cm^{-1} coinciding with changes from $Ru(OH_2)-Ru(OH_2)$ to $Ru(OH_2)-Ru(OH)$ to Ru(OH)−Ru(OH) (Figure 5). The Raman band at 319 cm^{-1} in the pH = 0 spectrum is due to a vibration of the buffer. For the chloro complex, ν_s(Ru−O−Ru) appears at 395 cm^{-1}. In the spectra of $[(bpy)_2(HO)Ru^{III}ORu^{IV}(OH)(bpy)_2]^{3+}$, and $[(bpy)_2ClRu^{III}ORu^{IV}Cl(bpy)_2]^{3+}$ major differences include new bands near 270 and 438 cm^{-1} compared to a single band at 433 cm^{-1} for $[(bpy)_2(H_2O)Ru^{III}ORu^{IV}(OH_2)(bpy)_2]^{5+}$ and $[(bpy)_2(H_2O)Ru^{III}ORu^{IV}(OH)(bpy)_2]^{4+}$. In the spectrum of the chloro complex, there is a band at 182 cm^{-1} compared to 175 cm^{-1} for the aqua complex. In the spectrum of the acetonitrile derivative $[(bpy)_2(CH_3CN)Ru^{III}ORu^{IV}(NCCH_3)(bpy)_2]^{5+}$, the Raman bands are narrower with ν_s(Ru−O−Ru) appearing at 384 cm^{-1}.

In Figure 6 are shown resonance Raman spectra of $[(bpy)_2(H_2O)Ru^{III}ORu^{IV}(OH)(bpy)_2]^{4+}$, $[(bpy)_2(H_2O)Os^{III}OOs^{IV}(OH_2)(bpy)_2]^{5+}$, and $[(tpy)(bpy)Os^{III}OOs^{IV}(bpy)(tpy)]^{5+}$ in H_2O buffered at pH = 1. The spectra of $[(bpy)_2(H_2O)Os^{III}OOs^{IV}(OH_2)(bpy)_2]^{5+}$ and $[(bpy)_2(H_2O)Ru^{III}ORu^{IV}(OH)(bpy)_2]^{4+}$ are similar, with ν_s(M−O−M) at 386 cm^{-1}, an intense band at 136 cm^{-1}, and ∼10 additional bands between 100 and 500 cm^{-1}. An intense band appears at 370 cm^{-1} for $[(tpy)(bpy)Os^{III}OOs^{IV}(bpy)(tpy)]^{5+}$ which is not observed for the Ru complexes. Additionally, Raman bands at 177, 211, 244, 314, and 350 cm^{-1} for $[(bpy)_2(H_2O)Os^{III}OOs^{IV}(OH_2)(bpy)_2]^{5+}$ are not present in the spectrum of $(tpy)(bpy)Os^{III}OOs^{IV}(bpy)(tpy)]^{5+}$.

In the spectra of the two $M^{III}OM^{IV}$−bpy complexes between 500 and 1000 cm^{-1}, Raman bands for bpy appear along with the first overtone and combinations of ν_s(M−O−M). The high-energy regions of these two spectra are dominated by bands from the ring vibrations of the bpy ligands. Some of the intensity near 760 and 1030 cm^{-1} arises from Raman bands of the buffer. The band energies from the Raman spectra of these complexes are presented in Table 5 with suggested assignments.

Discussion

One of the questions we hoped to address in this study was the change in structure that occurs in the μ-oxo core upon oxidation of $[(bpy)_2(H_2O)Ru^{III}ORu^{III}(OH_2)(bpy)_2]^{4+}$. Another was the structural effect of the loss of a proton induced by the increased acidity of the Ru^{IV}−aqua group upon oxidation of Ru^{III} (from $pK_a = 0.4$ to $pKa = 5.9$). Ultimately, the loss of both protons and electrons is a key in meeting the mechanistic demands of water oxidation, $2H_2O \rightarrow O_2 + 4H^+ + 4e^-$.

Oxidation to $Ru^{III}ORu^{IV}$ causes a decrease in Ru−O−Ru bond distances in $[(bpy)_2(H_2O)Ru^{III}ORu^{IV}(OH)(bpy)_2](ClO_4)_4$ (1.823 and 1.847 Å) compared to $[(bpy)_2(H_2O)Ru^{III}ORu^{III}(OH_2)(bpy)_2](ClO_4)_4 \cdot 2H_2O$ (1.869 Å). There is a structural asymmetry in the bridge which is expected, given the different coordination environments at the metal ions. The shorter bond distance to the Ru ion bound to the hydroxy ligand suggests an asymmetrical electronic distribution in the bridge consistent with the oxidation state distribution $(H_2O)Ru^{III}ORu^{IV}(OH)$. Even so, the Ru−N distances to the bpy ligands are not significantly different at the two Ru ions. The importance of Ru−O−Ru π bonding in the bridge is evident in comparing the Ru−O distances in the bridge to those of the terminal Ru−O of the aqua (2.148 Å) and hydroxyl (1.978 Å) ligands. The bond lengths in the bridge are significantly shortened compared to the more typical Ru−O single bond length for the aqua ligand.

Bond angles are also affected by electron content. The Ru−O−Ru angles in $[(bpy)_2(H_2O)Ru^{III}ORu^{IV}(OH)(bpy)_2](ClO_4)_4$ (170.0(7)°) and $[(bpy)_2ClRu^{III}ORu^{IV}Cl(bpy)_2](ClO_4)_3 \cdot H_2O$ (170.7(5)°) are very similar and larger than those for $[(bpy)_2(H_2O)Ru^{III}ORu^{III}(OH_2)(bpy)_2](ClO_4)_4 \cdot 2H_2O$ (165.4(3)°) and $[(bpy)_2(NO_2)Ru^{III}ORu^{III}(NO_2)(bpy)_2](ClO_4)_4 \cdot 2H_2O$ (157.2(3)°).[10]

In μ-oxo complexes of Fe^{III}, it has been suggested that the bridging angle is determined by a balance between the electronic preference for a particular conformation at the bridge and nonbonding repulsion between the ancillary ligands.[11] Hoff-

(10) Phelps, D. W.; Kahn, M.; Hodgson, D. J. *Inorg. Chem.* **1975**, *14*, 2486.

(11) Mukherjee, R. N.; Stack, T. D. P.; Holm, R. H. *J. Am. Chem. Soc.* **1988**, *110*, 1850.

Table 4. Raman Band Energies (cm^{-1}) with Excitation at 647.1 nm and Assignments of the Major Contributors to the Normal Modes[a]

$[(bpy)_2(L)Ru^{III}ORu^{III}(L)(bpy)_2]^{4+}$				$[(phen)_2(L)Ru^{III}ORu^{III}(L)(phen)_2]^{4+}$			
L = H_2O	L = OH^-	L = Cl^-	L = CH_3CN	L = H_2O	L = OH	L = CH_3CN	assignt
		120					
133 p	132	132 sh	132 p	129	130	133	δ_s(RuORu)
						161	
170 dp	170	172	174 dp				ν(bpy)
				180	180	182	ν(phen)
			202 dp				
213 dp	213	213					
						211	
239 p	239	240	241 p	236	236	240	
				247	247		
254	254	253					ν(bpy)
				267	267	269	
				292	292		
			286			288	
						295	
300 p	301	300 sh	296 p	306	306	310	ν_s(Ru−N)/ν_{19}(bpy)
					318	318	
329	329	329	326 sh				
				334	334		
				339	339	339	ν(phen)
343 dp	343	341	339 dp				ν(bpy)
368 sh, p	368 sh	368 sh	364 p	372 sh	372 sh	370	ν_{18}(bpy)
384 p	382	380	378 p	382	382	375	ν_s(RuORu)
400 sh	400 sh	400 sh		400 sh	400 sh		
419	419	421	419 dp				
				429	429	421	
438 dp	437	438	428 dp	435	435	437	
		441	441 dp				
				461	461	460	ν(phen)
468 p	468	468	467 p				ν(bpy)
				472	472		
485 p	486	486	484 p				
				495	495	496	
				523			ν(phen)
551				560			ν(phen)/ν_s(RuORu) + 170 (180)
				616			ν_s(RuORu) + 236
646				654			ν_s(RuORu) + 254 (267)
666							ν_{17}(bpy)
728							ν_s(RuORu) + 343
				750			ν(phen)
				760 br			$2\nu_s$(RuORu)
765							$2\nu_s$(RuORu), ν(bpy)
820 sh				820 sh			ν_{as}(RuORu)
				882			ν(phen)
1041							ν_{15}(bpy)
				1060			ν(phen)
1110				1111			ν_{13}(bpy),ν(phen)
1176							ν_{12}(bpy)
				1213			ν(phen)
1272							ν_{10}(bpy)
				1308			ν(phen)
1318							ν_9(bpy)
				1455			ν(phen)
1494							ν_7(bpy)
				1517			ν(phen)
1563							ν_6(bpy)
1607							ν_5(bpy)

[a] p and dp indicate polarized or depolarized band from depolarization ratio measurements. sh signifies a band present as a shoulder of a stronger band. The notation ν_x(bpy) is from: Strommen, D. P.; Mallick, P. K.; Danzer, G. D.; Lumpkin, R. S.; Kincaid, J. R. *J. Phys. Chem.* **1990**, *94*, 1357.

mann and co-workers have conducted molecular orbital calculations on Fe−O−Fe (d^5−d^5) systems and shown that a bond angle of less than 150° is favored when ligand interactions are not a factor.[12] In complexes of Ru, there is evidence for strong electronic coupling between Ru ions across the μ-oxo bridge and, as noted above, structural evidence for significant π bonding. A simple molecular orbital analysis predicts that mixing two sets of two dπ orbitals at each Ru^{III} with two p orbitals at the bridging O results in a lowest occupied set of two filled, largely O π orbitals, two filled nonbonding, largely dπ orbitals, n(dπ), and two half-filled antibonding orbitals, largely dπ in character, π*(dπ). Bending along the Ru−O−Ru axis removes the degeneracy of the antibonding orbitals, and double occupation of the lower of the two leads to an electronic stabilization. This tends to decrease the Ru−O−Ru bond angle toward 120° as found, for example, in $[(L)(acac)Ru^{III}ORu^{III}(acac)(L)](PF_6)_2$ (L is 1,4,7-trimethyl-1,4,7-triazacyclononane; acac is pentane-2,4-dionate).[13]

(12) Tatsumi, K.; Hoffmann, R. *J. Am. Chem. Soc.* **1981**, *103*, 3328.

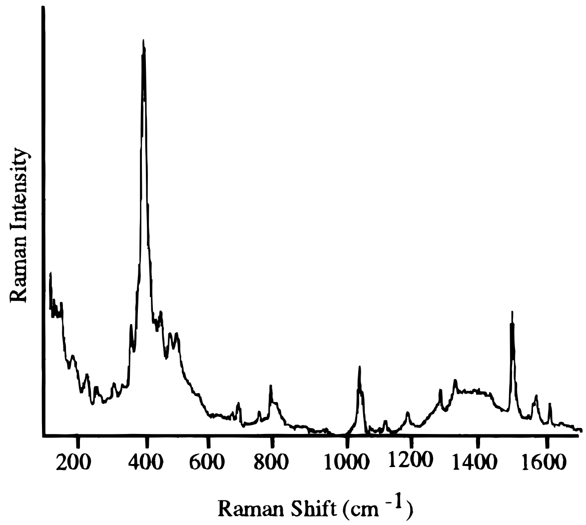

Figure 4. Resonance Raman spectrum of $[(bpy)_2(H_2O)Ru^{III}ORu^{III}(OH_2)(bpy)_2]^{4+}$ in H_2O/triflic acid, pH = 1, from 100 to 1700 cm^{-1}. The spectrum was measured with 514.5 nm excitation.

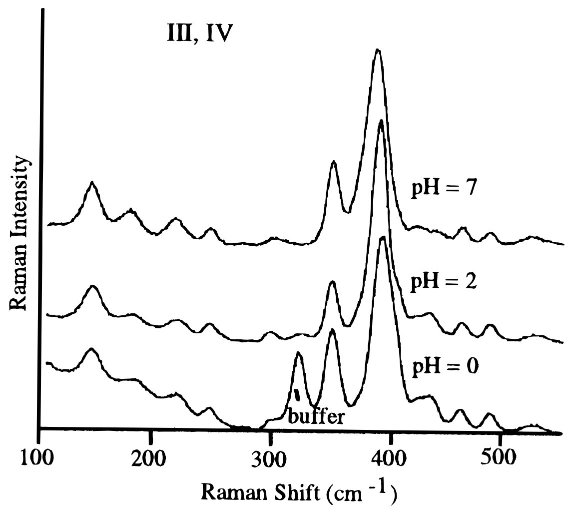

Figure 5. Resonance Raman spectra of $[(bpy)_2(H_2O)Ru^{III}ORu^{IV}(OH_2)(bpy)_2]^{5+}$ (pH = 0), $[(bpy)_2(H_2O)Ru^{III}ORu^{IV}(OH)(bpy)_2]^{4+}$ (pH = 2) and $[(bpy)_2(HO)Ru^{III}ORu^{IV}(OH)(bpy)_2]^{+}$ (pH = 7).

If two or more electrons are removed from a d^5-d^5 ion, a linear conformation is favored. A linear geometry has been observed for all μ-oxo complexes of electronic configuration d^n-d^n with $n < 5$. Examples are $[(NH_3)_5CrOCr(NH_3)_5]Cl_4\cdot H_2O$ (d^3-d^3), $K_4[Cl_5RuORuCl_5]H_2O$ (d^4-d^4), and $K_4[Cl_5OsOOsCl_5]$-H_2O (d^4-d^4).[14] In these cases, the π^* levels resulting from the bridged-based interactions are empty. There is no longer an electronic basis for bending, and a linear geometry is preferred to minimize nonbonding ligand repulsions. In the d^5-d^4 salts $[(bpy)_2(H_2O)Ru^{III}ORu^{IV}(OH)(bpy)_2](ClO_4)_4$, $[(bpy)_2ClRu^{III}ORu^{IV}Cl(bpy)_2](ClO_4)_3\cdot H_2O$, and $[(tpy)(bpy)Os^{III}OOs^{IV}(bpy)(tpy)]Na(ClO_4)_6\cdot 3H_2O$, the M−O−M bond angle is ∼170°, a compromise between linearity and the smaller angle observed in $[(bpy)_2(H_2O)Ru^{III}ORu^{III}(OH_2)(bpy)_2](ClO_4)_4\cdot 2H_2O$, for example. The intermediate structure probably represents a balance between electronic stabilization derived from the bridge interaction and repulsive interactions between the nonbridging ligands. The decrease in electronic occupation in the antibonding π^*-($d\pi$) bridge orbitals also appears in the shortened Ru−O length in the bridge.

(13) Schneider, R.; Weyhermuller, T.; Wieghardt, K.; Nuber, B. *Inorg. Chem.* **1993**, *32*, 4925.
(14) Campbell, J. R.; Clark, R. J. H. *Mol. Phys.* **1978**, *36*, 1133.

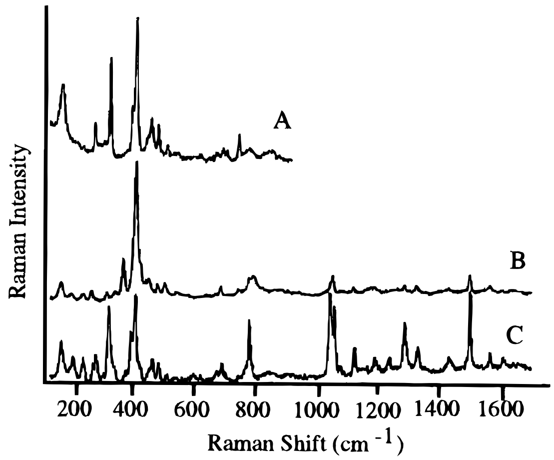

Figure 6. Resonance Raman spectra of (A) $(tpy)(bpy)Os^{III}OOs^{IV}(bpy)(tpy)]^{5+}$ (pH = 1) from 100 to 900 cm^{--1}, (B) $[(bpy)_2(H_2O)Ru^{III}ORu^{IV}(OH)(bpy)_2]^{4+}$ (pH = 2), and (C) $[(bpy)_2(H_2O)Os^{III}OOs^{III}(OH_2)(bpy)_2]^{5+}$ (pH = 0) between 100 and 1700 cm^{-1}. The spectra were measured with 514.5 nm excitation at room temperature. Raman band energies are listed in Table 5.

Table 5. Raman Band Energies (cm^{-1}) with 514.5 nm Excitation for $[(bpy)_2(H_2O)Ru^{III}ORu^{IV}(OH)(bpy)_2]^{4+}$ ($Ru^{III}ORu^{IV}$), $[(bpy)_2(H_2O)Os^{III}OOs^{IV}(OH_2)(bpy)_2]^{5+}$ ($Os^{III}OOs^{IV}$), and $[(tpy)(bpy)Os^{III}OOs^{IV}(bpy)(tpy)]^{5+}$ in H_2O/Triflic Acid, pH = 1, with Proposed Assignments of the Major Contributor to the Normal Mode

$Ru^{III}ORu^{IV}$	$Os^{III}OOs^{IV}$	$(tpy)(bpy)Os^{III}$-$OOs^{IV}(bpy)(tpy)]^{5+}$	assignt
136	136	138	δ_s(MOM)
174	177		
214	210		
242	245		
250 sh	254	249	ν(bpy)
294	297	300	ν_s(M−N), ν_{19}(bpy)
321	314		
348	350		
370 sh	371	372	ν_{18}(bpy)
389	385	386	ν_s(MOM)
404 sh	400 sh		
423	432	425	
433	441	437	
461	463	459	ν(bpy)
486	491	489	
525	518	520	ν_s(MOM) + 136
	580		
670	674	677	ν_{17}(bpy)/ν(tpy)
		689	ν_s(MOM) + 300
		728	ν(tpy)
734			ν_s(MOM) + 348
764	765		ν_{16}(bpy)/triflate
777	770 br	770 br	2(ν_s(MOM))
790	836	830	ν_{as}(MOM)
822			ν_s(MOM) + 433
847	850		ν_s(MOM) + 461(463)
868	865		ν_s(MOM) + 486(491)
	1032		triflate
1042	1046		ν_{15}(bpy)
1109	1113		ν_{13}(bpy)
1164			
1175	1179		ν_{12}(bpy)
	1229		
1280	1279		ν_{10}(bpy)
1318	1322		ν_9(bpy)
1426	1425		
1496	1498		ν_7(bpy)
1564	1564		ν_6(bpy)
1605	1607		ν_5(bpy)

The structural changes that are observed are relevant to the possible role of the bridge in water oxidation. The tendency toward linearity presumably leads to a linear bridge for the higher oxidation states $Ru^{IV}-O-Ru^{IV}$ (d^4-d^4) through Ru^V-O-Ru^V (d^3-d^3). It is already apparent in oxidation of $Ru^{III}-O-Ru^{III}$ to $Ru^{III}-O-Ru^{IV}$ by the increase in Ru−O−Ru bond angle. Oxidation causes other changes as well. One is the increase in the $H_2O-Ru-O$ angle from 89.4(2)° in $[(bpy)_2(H_2O)Ru^{III}ORu^{III}(OH_2)(bpy)_2](ClO_4)_4 \cdot 2H_2O$ to 94.7(5)° for $H_2O-Ru-O$ and 99.2(5)° for O−Ru−OH in $[(bpy)_2(H_2O)Ru^{III}ORu^{IV}(OH)(bpy)_2](ClO_4)_4$. This causes a bending *away* of the O atoms cis to the bridge. This is caused by increased nonbonding, electron−electron repulsion between OH^- and H_2O compared to H_2O and H_2O and between these groups and the Ru−O−Ru bridge. In the higher oxidation state $Ru^{IV}-O-Ru^V$ and Ru^V-O-Ru^V forms, considerable nonbonded electron−electron repulsion is expected between π-bonded Ru−oxo groups across the μ-oxo bridge and between the π electrons of the oxo group and those of the μ-oxo bridge. This presumably leads to relatively large O−Ru−O angles and an increase in the O···O separation distance across the bridge.

The O···O separation distance depends on both the Ru−O−Ru bridge angle and the O−Ru−Ru−O torsional angle. In $[(bpy)_2(H_2O)Ru^{III}ORu^{III}(OH_2)(bpy)_2](ClO_4)_4 \cdot 2H_2O$ the O···O distance is 4.725(5) Å and the O−Ru−Ru−O torsional angle 65.7°. In $[(bpy)_2(H_2O)Ru^{III}ORu^{IV}(OH)(bpy)_2](ClO_4)_4$, the O···O distance is 5.555(18) Å and the torsional angle 117.2°. At least for $Ru^{III}-O-Ru^{III}$ there is no obvious electronic effect dictating the magnitude of the torsional angle. In the diammine complex $[(bpy)_2(NH_3)Ru^{III}ORu^{III}(NH_3)(bpy)_2](ClO_4)_4$, the angle is 28.45°. It is ~0° in $[(bpy)_2(NH_3)Ru^{III}ORu^{III}(OH)(bpy)_2](ClO_4)_3$.[15,16]

On the basis of this analysis, oxidation past $Ru^{III}-O-Ru^{IV}$ is expected to lead to a linear Ru−O−Ru array. In oxidation states $Ru^{IV}-O-Ru^V$ (d^4-d^3) and Ru^V-O-Ru^V (d^3-d^3), linear structures can be predicted with cis-oxo groups bent significantly away from the μ-oxo core and O=Ru−O angles exceeding 90°. Nevertheless, an appropriate combination of torsional rotation around the Ru−O−Ru axis and bending of the oxo groups toward each other along the Ru−O−Ru axis would provide a basis for O−O coupling and O_2 formation. These motions define the reaction coordinate for one of the pathways proposed for O_2 evolution from Ru^V-O-Ru^V.[5]

There is evidence for strong electronic coupling across the μ-oxo bridge in the short Ru−O bond distances, and an additional question of interest is the electronic distribution in the mixed-valence ions. Specifically, in $Ru^{III}-O-Ru^{IV}$ is the appropriate oxidation state description $M^{III}-O-M^{IV}$ with localized oxidation states (class II in the Robin and Day scheme) or $M^{III.5}-O-M^{III.5}$ with delocalized oxidation states?[17]

Because the difference in proton content induces a coordination asymmetry, it is not possible to address this question in $[(bpy)_2(H_2O)Ru^{III}ORu^{IV}(OH)(bpy)_2]^{4+}$, but it can be addressed in $[(bpy)_2ClRu^{III}ORu^{IV}Cl(bpy)_2](ClO_4)_3 \cdot H_2O$. In this ion, the Ru−Cl bond distances are 2.357 and 2.339 Å and the Ru atom with the shorter Ru−Cl bond also has the shorter Ru−O(bridge) bond distance (1.805(9) vs 1.845(9) Å). These structural differences point to an asymmetrical electronic distribution, at least, in the solid state. The difference between the two Ru−Cl bond distances ($\Delta = 0.018$ Å) is smaller than in other oxidation state comparisons. The average difference between $[Ru^{III}(bpy)_2Cl_2]Cl$ (2.322 and 2.328 Å) and $[Ru^{II}(bpy)_2Cl_2]$ (2.426 Å) is 0.102 Å. There may be localized oxidations states in $[(bpy)_2ClRu^{III}ORu^{IV}Cl(bpy)_2]^{3+}$, but electronic delocalization across the μ-oxo bridge is extensive. The same issue arises for $[(tpy)(bpy)Os^{III}OOs^{IV}(bpy)(tpy)]Na(ClO_4)_6 \cdot 3H_2O$. In this case, the Os−O−Os angle (169.0°) is near 170° and there is structural asymmetry in the Os−O bridge bonds. The difference in Os−O bond lengths ($\Delta = 0.016$ Å) is considerably less than in $[(bpy)_2ClRu^{III}ORu^{IV}Cl(bpy)_2]^{3+}$ ($\Delta = 0.040$ Å). This may be a consequence of a greater degree of mixing and electronic delocalization for Os.

Resonance Raman Spectra. Resonance Raman spectroscopy has been extensively utilized in the study of μ-oxo complexes. Measurements on $[Cl_5RuORuCl_5]^{4-}$ and related ions have revealed spectra which include multiple overtone and combination progressions.[14] μ-Oxo iron complexes have been studied as models for the binuclear iron sites in hemerythrin and ribonucleotide reductase.[18]

Absorption spectra of $M^{III}-O-M^{III}$ (M = Ru, Os) complexes include a characteristic, high-absorptivity band in the region 600−700 nm with an additional band appearing between 350 and 450 nm. Excitation into the lower energy band results in significant enhancement of the M−O−M symmetric stretch (ν_s(M−O−M)). A bent M−O−M structure is predicted to have three Raman-active modes, ν_s(M−O−M), an asymmetric M−O−M stretch (ν_{as}(M−O−M)), and a symmetric M−O−M deformation (δ_s(M−O−M)), with ν_s(M−O−M) the most intense. Scattering from $[(bpy)_2(H_2O)Ru^{III}ORu^{III}(OH_2)(bpy)_2]^{4+}$ following higher energy excitation (e.g. Figure 4) reveals that ν_s(M−O−M) is less enhanced and the pattern of enhanced ν(bpy) bands is similar to those enhanced upon scattering from metal-to-ligand charge transfer (MLCT) excitation of $[Ru^{II}(bpy)_3]^{2+}$ and related polypyridyl complexes.[19] These observations are consistent with a MLCT origin for the higher energy band.[20]

Hurst and co-workers have applied resonance Raman spectroscopy to $[(bpy)_2(H_2O)Ru^{III}ORu^{III}(OH_2)(bpy)_2]^{4+}$ and higher oxidation states.[6] With ^{18}O substitution at the bridge, ν_s(Ru−O−Ru) was definitively identified as an intense Raman feature between 370 and 400 cm^{-1} in the various oxidation states of the dimer. The data were interpreted as being consistent with a change toward a linear structure in the higher oxidation states. Some questions remain concerning the identification of the higher oxidation state forms.[21]

To gain further insight on Raman assignments, infrared spectra were also acquired. The infrared spectrum of $[(bpy)_2(H_2O)Ru^{III}ORu^{III}(OH_2)(bpy)_2](ClO_4)_4 \cdot 2H_2O$ between 400 and 1000 cm^{-1} as a KBr pellet includes bands at 421, 625, 650, 666, 733, 774, 810, 900, and 965 cm^{-1}. The bands at 421, 650, 666, 733, 774, 900, and 965 cm^{-1} can be attributed to bpy vibrations. The intense band at 625 cm^{-1} is a ClO_4^- band which leaves the 810 cm^{-1} band to be assigned as ν_{as}(Ru−O−Ru). In the Raman spectrum of $[(bpy)_2(H_2O)Ru^{III}ORu^{III}(OH_2)(bpy)_2]^{4+}$, a band appears near 820 cm^{-1} which is presumably ν_{as}(Ru−O−Ru).

Following incubation of $[(bpy)_2(H_2O)Ru^{III}ORu^{III}(OH_2)(bpy)_2]^{4+}$ in D_2O and $H_2{}^{18}O$, there were no substantial Raman band shifts. Difference spectra reveal slight shifts (2 −3 cm^{-1}) in ν_s(Ru−O−Ru) and changes in regions of the spectrum where $2\nu_s$(Ru−O−Ru) and ν_{as}(Ru−O−Ru) appear. No single Raman

(15) Ishitani, O.; White, P. S.; Meyer, T. J. *Inorg. Chem.* **1996**, *35*, 2167.
(16) Ishitani, O.; White, P. S.; Meyer, T. J. Unpublished results.
(17) (a) Robin, M. B; Day, P. *Adv. Inorg. Chem. Radiochem.* **1967**, 10. (b) Creutz, C. *Prog. Inorg. Chem.* **1983**, *30*, 1.
(18) (a) Solbrig, R. M.; Duff, L. L.; Shriver, D. F.; Klot, I. M. J. *Inorg. Biochem.* **1982**, *17*, 69. (b) Plowman, J. E.; Loehr, T. M.; Schauer, C. K.; Anderson, O. P. *Inorg. Chem.* **1984**, *23*, 3553. (c) Loehr, T. M.; Shiemke, A. K. In *Resonance Raman Spectra of Heme and Metalloproteins*; Spiro, T. G., Ed.; Biological Applications of Raman Spectroscopy, Vol. 3; Wiley and Sons: New York, 1988; p 439.
(19) Strommen, D. P.; Mallick, P. K.; Danzer, G. D.; Lumpkin, R. S.; Kincaid, J. R. J. *Phys. Chem.* **1990**, *94*, 1357.
(20) Graff, D.; Omberg, K. Unpublished results.
(21) Chronister, C.; Binstead, R.; Devenney, M. Work in progress.

band can be assigned to a symmetrical Ru−OH_2 stretch, which is unfortunate, since this would be an important vibration to monitor in the oxidation chemistry. Similarly, replacement of H_2O with hydroxide, chloride, or acetonitrile led to no changes in the Raman spectra which could suggest an assignment for ν(Ru−L) (L = H_2O, hydroxide, chloride, or acetonitrile).

The absorption bands in the 600−700 nm region are assigned to n(dπ) → π*(dπ) transitions of the Ru−O−Ru bridge.[7] The absence of enhancements for ν_s(Ru−L) (L = H_2O, OH^-, Cl^-, CH_3CN) shows that they are, at best, weakly coupled to this transition. In spectra acquired with MLCT excitation (457.9 nm) of $[Ru^{II}(tpy)(bpy)(OH_2)]^{2+}$, there was no change in Raman bands below 600 cm^{-1} upon incubation of the complex in $H_2{}^{16}O$, $H_2{}^{18}O$, or $D_2{}^{16}O$. Bands appear at 249, 292, 318, 376, 443, 463, 476, 500, and 542 cm^{-1}, reminiscent of the abundance of Raman bands in this region for the μ-oxo complexes.

Given the absence of definitive conclusions from the isotope studies, no Raman bands below 500 cm^{-1} can be definitively assigned to δ_s(Ru−O−Ru) or ν_s(Ru−OH_2). The numerous vibrations in this region can be viewed as highly mixed with normal modes formed from local modes of the Ru−O−Ru bridge, ν_s(Ru−OH_2), and the bpy or phen ligands. From the depolarization ratio measurements (Table 4) the bands at 133, 239, and 300 cm^{-1} in the spectrum of $[(bpy)_2(H_2O)Ru^{III}ORu^{III}(OH_2)(bpy)_2]^{4+}$ are totally symmetrical vibrations and may contain contributions from the symmetrical Ru−O−Ru deformation or the symmetrical Ru−OH_2 stretch.

In the infrared spectrum of $[(bpy)_2(H_2O)Ru^{III}ORu^{IV}(OH)(bpy)_2](ClO_4)_4$ in a KBr pellet, bands appear analogous to those in the spectrum of $[(bpy)_2(H_2O)Ru^{III}ORu^{III}(OH_2)(bpy)_2](ClO_4)_4\cdot 2H_2O$ which can be assigned to perchlorate or bpy vibrations. The band analogous to ν_{as}(Ru−O−Ru) at 810 cm^{-1} for $[(bpy)_2(H_2O)Ru^{III}ORu^{III}(OH_2)(bpy)_2](ClO_4)_4\cdot 2H_2O$ is shifted to 796 cm^{-1}, showing that there is a slight shift to lower energy for this band upon oxidation.

From the Raman data for the Ru^{III}−O−Ru^{IV} complexes, ν_s(Ru−O−Ru) appears as an intense band near 390 cm^{-1} for all derivatives. Again, no single band can be attributed to ν_s(Ru−L) (L = OH_2, OH^-, Cl^-, CH_3CN) or δ_s(Ru−O−Ru) on the basis of spectral changes as L is varied. As in $Ru^{III}ORu^{III}$, internal ligand modes likely contribute to these bands and the normal modes are highly mixed. Incubation of $[(bpy)_2(H_2O)Ru^{III}ORu^{IV}(OH)(bpy)_2]^{4+}$ in D_2O or $H_2{}^{18}O$ causes a slight shift in ν_s(Ru−O−Ru). A small change is also noted in the Raman band at 349 cm^{-1}, which could suggest some Ru−L character in this band. Slight changes also occur in the difference spectrum near 800 cm^{-1}, consistent with a slight shift in ν_{as}(Ru−O−Ru).

Resonance Raman spectra of $[(tpy)(bpy)Os^{III}OOs^{IV}(bpy)(tpy)]^{5+}$ and $[(bpy)_2(H_2O)Os^{III}OOs^{IV}(OH_2)(bpy)_2]^{5+}$ acquired with 514.5 nm excitation add additional insight. Both bpy and tpy bands are enhanced relative to the intense ν_s(M−O−M) band. There is presumably considerable MLCT overlap with n(dπ) → π*(dπ) (Os−O−Os) in this excitation region. Bands at 249 and 372 cm^{-1}, which have significant bpy character, are especially enhanced, particularly in the spectrum of $[(tpy)(bpy)Os^{III}OOs^{IV}(bpy)(tpy)]^{5+}$. An intense band appears at 138 cm^{-1}. This band and the totally symmetrical bands for the Ru oxo complexes in the same region may have significant δ_s(M−O−M) character resonantly enhanced by n(dπ) → π*(dπ) excitation. A intense band at 300 cm^{-1} is reasonably assigned to a mode predominantly ν_s(Os-N) in character but mixed with internal bpy motions. A related band appears near 300 cm^{-1} for the Ru−bpy complexes in Table 4. These tentative assignments leave the 239-cm^{-1} band for Ru^{III}−O−Ru^{III} the one remaining, unassigned symmetrical stretch in the low-energy region of the spectrum. This band does not substantially change with isotopic or ligand substitution. All isotope studies were conducted by incubation of the complex in the appropriate buffer; synthesis of specifically labeled complexes will assist in definitive assignments.

The assignments of ν_s(M−O−M), ν_{as}(M−O−M), and ν_s(M-N) and the tentative assignment of δ_s(M−O−M) will be important in the characterization of the higher oxidation states of the water oxidation catalyst. Monitoring these Raman bands as a function of oxidation state will provide structural details for the higher oxidation states where it will not be possible to obtain crystal structures. The comparison of the structural data for Ru^{III}−O−Ru^{III} and Ru^{III}−O−Ru^{IV} demonstrates a change toward linear geometry upon oxidation, which is reflected in the Raman spectra. Additionally, resonance Raman excitation profiles will allow a probe of differences in electronic structure between oxidation states.

Acknowledgment. This work was supported National Institutes of Health Grant 5-R01-GM32296-11 to T.J.M. Support from the Laboratory Directed Research and Development Program at Los Alamos National Laboratory to J.R.S. is also acknowledged.

Supporting Information Available: Tables listing complete crystal data and structure solution and refinement conditions, atomic coordinates, bond distance and angles, and thermal parameters (7 pages). Ordering information is given on any current masthead page. Structure factor tables may be obtained directly from the authors.

IC960348O